Characterization and Parametric Optimization of Performance Parameters of DLC-Coated Tungsten Carbide (WC) Tool Using TOPSIS

Ramakant Rana [1,2,*] , **R. S. Walia** [3] **and Qasim Murtaza** [2]

1   Department of Mechanical and Automation Engineering, Maharaja Agrasen Institute of Technology,
     Delhi 110086, India
2   Department of Mechanical Engineering, Delhi Technological University, Delhi 110042, India;
     qasimmurtaza@dce.ac.in
3   Department of Production and Industrial Engineering, Punjab Engineering College,
     Chandigarh 160012, India; waliaravinder@yahoo.com
*   Correspondence: ramakantrana@gmail.com

Abstract: In this work, we have deposited the diamond-like carbon (DLC) coating on the tungsten carbide (WC) tool insert using the thermal chemical vapor deposition (CVD) method. For the growth of DLC coating, sugarcane bagasse was used as a carbon precursor. Raman spectroscopy, a field emission scanning electron microscope (FESEM), and X-ray diffraction (XRD) were used to confirm the presence of DLC coating on the tungsten carbide tool inserts. The hardness tests were also performed for inspecting the microhardness induced by the self-developed DLC coating on the tungsten carbide (WC) tool insert. To determine the optimum process parameters for the turning operation on an aluminum (6061) workpiece using a self-developed DLC-coated tungsten carbide (WC) tool insert, we have applied the technique for order preference by similarity to ideal solution (TOPSIS) methods. The process parameters considered for the optimization were feed rate, cutting speed, and depth of cut. Whereas chosen response variables were flank wear, temperature in the cutting zone, and surface roughness. TOPSIS is utilized to analyze the effects of selected input parameters on the selected output parameters. This study in this paper revealed that it was advantageous to develop the DLC coating on the tungsten carbide tool inserts for the machining applications. The results also revealed that a 0.635 mm depth of cut, feed rate of 0.2 mm/rev, and cutting speed of 480 m/min were the optimum combination of process parameters.

Keywords: characterization; DLC coating; tungsten carbide; TOPSIS

1. Introduction

Day by day, there has been a huge demand for better and long-life tools used in the manufacturing industry. These tools are required for the machining of various hard materials like metal-based composites and aluminum–silicon-based alloys because of their extensive use in automobile and aerospace industries [1,2]. It is a challenge to achieve extreme tolerances with operations of high volume for these materials as they are difficult to machine using conventional cutting tools [3,4]. Diamond or diamond-like carbon (DLC)-coated tungsten carbide (WC) tools are ideal for machining hard materials due to their first-class wear resistance properties. Furthermore, DLC-coated WC tools have a proven track record of providing a good surface finish to the machined parts. The better finish of the surface is due to their chemical inertness and low coefficient of friction (COF), which is advantageous for lots of applications [5,6]. Diamond is an allotrope of the carbon, which has drawn a lot of constructive involvement in various fields of engineering and technology, undischarged to its technological applications and prominent underlying properties. In short, the diamond is least compressible and very hard. It has the most prominent thermal

conductivity at room temperature amongst all the available materials. Diamond also is very resistive to the corrosion caused by chemicals [7,8]. The use of the thermal chemical vapor deposition (CVD) technique for the growth of DLC films on the tungsten carbide (WC) substrates for its potential applications in the field of engineering has attracted considerable attention from earlier to recent years [9–11]. The thermal chemical vapor deposition technique has several advantages like a comparatively uncomplicated set-up, ease of operation, uniformity over a large area, and adaptability to all geometries [12]. The toughness of WC gets combined with the hardness of the coating by depositing the thin films of DLC on the WC substrates. This deposition results in a prominent property of wear resistiveness. Moreover, the DLC's thermal conductivity deeds as an additional safeguard for better heat conductivity. This quality of DLC coating maintains the lower temperature of the tool while machining by rapidly dissipating heat [13,14].

The cutting tool industry uses DLC films on WC cutting due to its resplendent properties like high thermal conductivity, high hardness, and high resistance to wear along with a low coefficient of friction [15]. Nevertheless, DLC films with high adhesive property are still a task because of its graphitization issue at the interface [16,17]. The reason for considering this thermal CVD method was that it uses sugarcane bagasse as a carbon precursor for the growth of DLC or diamond films [18,19]. Pyrolysis of sugarcane bagasse produces effluent gases having good thermal dissociation, which produces the thermodynamic equilibrium as well as the right chemical for diamond formation [19,20]. It is an important issue to assess the multi-responses concurrently in machining applications. To solve multi-response problems efficiently and appropriately, we can use TOPSIS as it is a simple procedure and a multi-objective optimization method. Rao [21] in his study of turning operations for evaluating machinability, used a combination of AHP and TOPSIS methods. Few researchers have used TOPSIS methods to optimize the machining parameters in their study for the turning operation [22,23]. They also looked into the surface morphology of the coated tools [24]. Adalarasan and Sundaram (2015) optimized the process parameters of their friction welding study while integrating two methods viz. GRA and Taguchi methods and revealed the effectiveness of the approach through their results [25].

On the basis of the above-mentioned literature, it has been found that limited researchers have reported the application of the TOPSIS method for the application of coated tools in the turning process. Therefore, in this paper, we have tried to estimate and optimize the selected input parameters using the self-developed DLC-coated tungsten carbide (WC) tool insert on the turning process. Raman spectroscopy, field emission scanning electron microscope (FESEM), and X-ray diffraction (XRD) along with energy-dispersive X-ray spectroscopy (EDaX) were used to characterize the as-developed DLC coating films on the WC inserts. In addition, the microhardness tests were also carried on the developed samples to manifest the potential advantage of coated tungsten carbide (WC) substrates for high wear resistance applications.

2. Materials and Methods

This section provides the precise details of the development of DLC coating on the tungsten carbide (WC) tool inserts along with the process of turning in machining operations.

2.1. Coating Method

Tungsten carbide (WC) inserts were used as a substrate material for the coating process. In the present work, DLC coatings were coated on the tungsten carbide tools inserts at atmospheric pressure using the thermal chemical vapor deposition (CVD) technique. The substrates were cleaned (pretreated) using a standard cleaning process with hydrofluoric (HF) acid and acetone ((CH_3)$_2$CO) for 7–10 min before depositing the film. Simultaneously, sugarcane bagasse (SBg) was used to produce pyrolyzed sugarcane bagasse (p-SBg) by placing sugarcane bagasse (SBg) in the split furnace set on a controlled temperature of 550 °C at atmospheric pressure for half an hour [18]. The activated carbon was produced from the pyrolyzed sugarcane bagasse (p-SBg) after chemical treatment [18,26]. After that,

the cleaned substrates of the tungsten carbide tool inserts and produced activated carbon were loaded in the reaction chamber of the thermal CVD system for the growth of the DLC coating. This process of the coating was carried out at atmospheric pressure in the thermal CVD system at ~900 °C. Sugarcane bagasse was used as a carbon precursor for the growth of DLC coating on the tungsten carbide (WC) tool inserts along with a mixture of Ar/H_2 in the ratio of 2:1 to carry the effluent gases and to remove the presence of oxygen in the reactor chamber of the thermal CVD process. Pyrolysis of sugarcane bagasse produces effluent gases which have good thermal dissociation. This thermal dissociation produces the right chemical and thermodynamic equilibrium, which is further responsible for the growth of DLC coating [18,20]. In the process, the deposition rate was found to be ~60 μm/h and the deposition time for the coating process was 10 min. As the deposition time was 10 min hence, the coating was having the thickness in the range of 8–10 μm. Experimental conditions for the deposition have been depicted in Table 1. Figure 1 depicts the process conditions which were used for developing the films from the pyrolysis process of sugarcane bagasse on the tungsten carbide tool insert substrate [20,22]. There is a high commercial value of the activated carbon in industry and it may be used for the removal of chlorine as well [20,27,28].

Table 1. Parameters and their values for the deposition of DLC coating.

S. No.	Parameters	Values
1	Method	Thermal chemical vapor deposition (CVD)
2	Material for producing coating	Activated carbon produced from p-SBg
3	Rate of growth	~60 μm/h
4	Time of deposition	8–10 min
5	Gas supplied	Ar/H_2 (2:1)
6	Surface pre-treatment	Hydrofluoric (HF) acid + acetone
7	Reaction chamber	35 mm quartz transparent tube
8	Pressure	1.013×10^5 Pa (atmospheric pressure)
9	Temperature	~900 °C

2.2. Turning Process

A Harrison make L-140 precision lathe was used to perform the cutting operation on the aluminum (6061) rod. The precision lathe had 3 jaw chucks to hold the workpiece. The process of machining is shown in Figure 2. A Fluke make Ti 400 thermal imaging camera (Fluke Ti 400, Everett, WA, USA) was used to capture the temperature in the cutting zone [29]. The use of the thermal imaging camera along with the output images are shown in Figure 3. Figure 3a is showing the output thermal image, whereas Figure 3b is depicting the image of the DLC-coated cutting tool under the turning process. A graph of temperature variation for the cutting tool at its contact point and its surroundings is shown in Figure 3c. Feed (*f*), cutting speed (V_c) and depth of cut (DOC), was selected as the input variables for the machining process [30,31]. The levels of the selected input parameters are shown in Table 2. The temperature in the cutting zone (Tc), surface roughness (Ra), and flank wear (Wf) were selected as the performance indicators (response variables) [32,33]. Table 3 shows the units and abbreviation of these response variables.
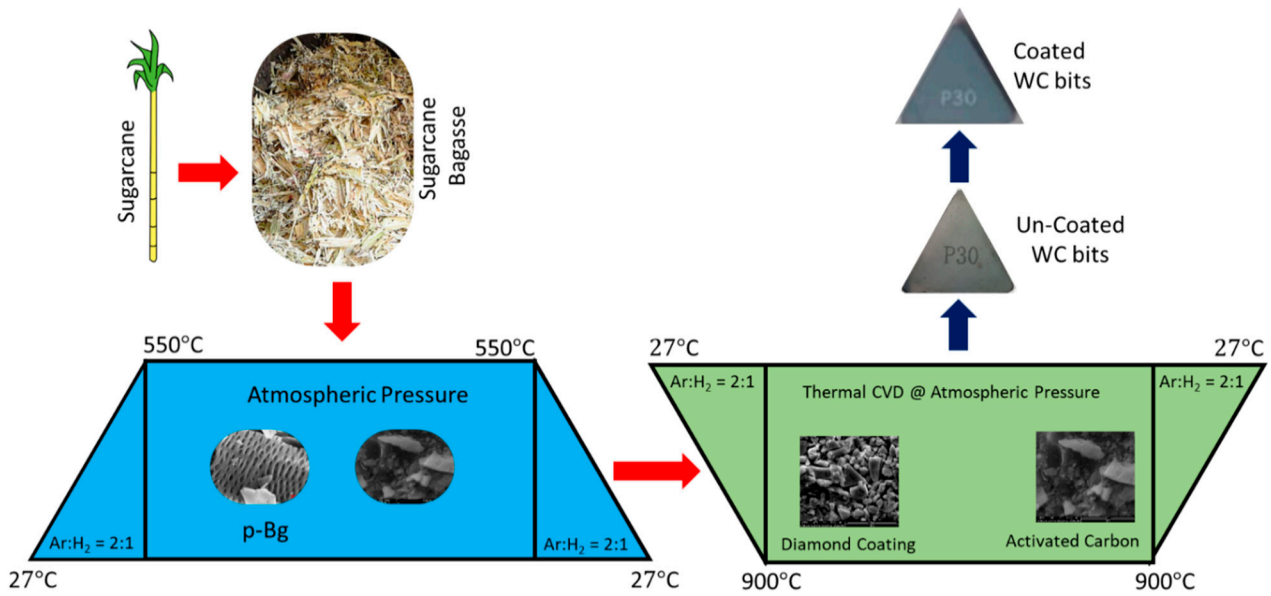
Figure 1. Process used for thermal chemical vapor deposition of DLC coating from pyrolysis of sugarcane bagasse [18,20,26].

Table 2. Levels of input parameters.

S. No.	Input Parameters	Unit	Level 1	Level 2	Level 3
1	Feed (f)	mm/rev	0.125	0.250	0.375
2	Cutting speed (Vc)	m/min	480	600	720
3	Depth of cut (DOC)	mm	0.375	0.635	0.895

Table 3. Selected response variables.

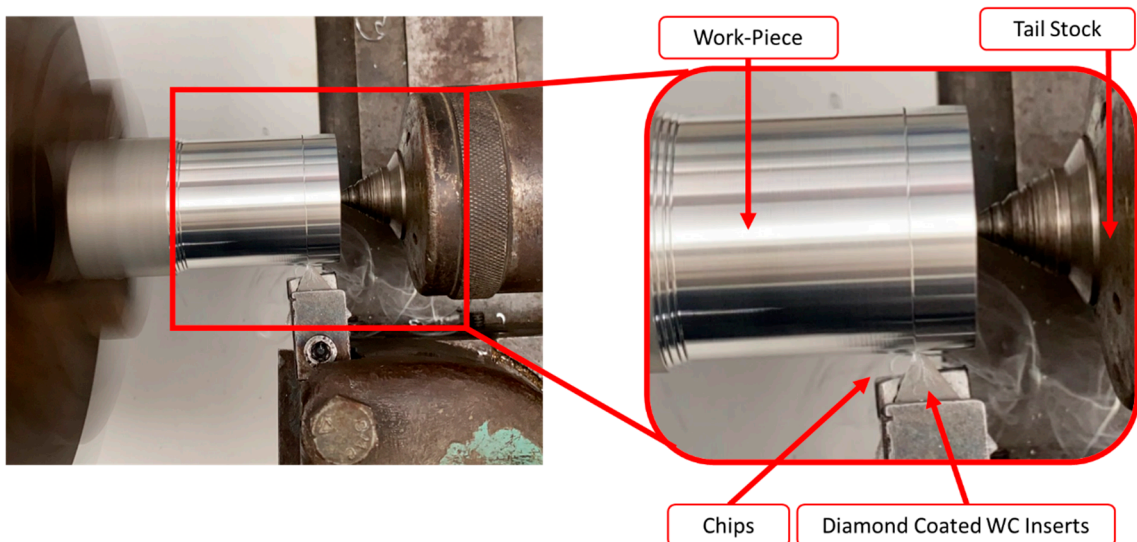| S. No.	Response Variables	Unit	Abbreviation
1	Temperature in the cutting zone	°C	Tc
2	Surface roughness	μm	Ra
3	Flank wear	μm	Wf

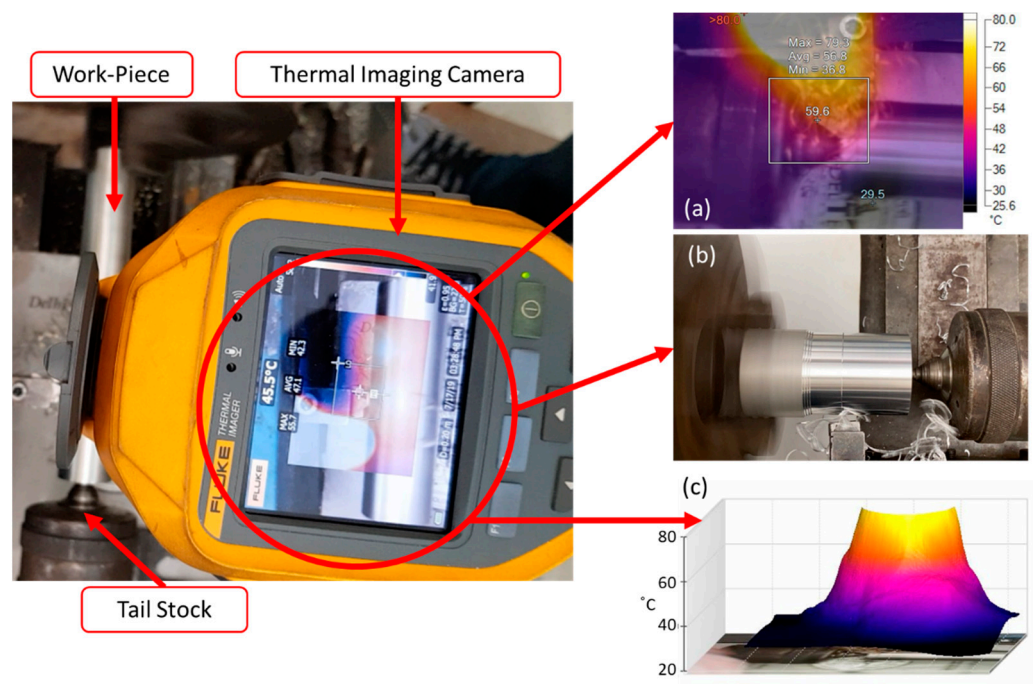**Figure 2.** Turning process using self-developed DLC-coated tungsten carbide (WC) tool insert.

Figure 3. Thermal imaging camera under the process of taking the thermal images; (**a**) thermal image of the cutting tool at its contact point, (**b**) image of DLC-coated cutting tool under the turning process and (**c**) graph of temperature variation for the cutting tool at its contact point and its surroundings.

3. Characterization

This section provides concise and precise details of the characterization of the self-developed DLC-coated tungsten carbide (WC) tool inserts.

3.1. EDaX and XRD Analysis

A Hitachi brand tabletop scanning electron microscope TM3000 was used to perform energy-dispersive X-ray spectroscopy (EDaX) on the un-coated samples of tungsten carbide (WC) tool inserts for identifying the elemental composition. The elemental composition and EDaX spectrum of the un-coated tungsten carbide (WC) substrate sample is shown in Table 4 and Figure 4, respectively.

A stereo microscopic image of the worn out DLC-coated tungsten carbide (WC) insert is shown in Figure 5 along with the SEM image. The elemental composition and EDaX spectrum of the worn-out surface of the DLC-coated tungsten carbide (WC) insets are shown in Figure 6 and Tables 5 and 6. The region at the red cross of Figure 6 is depicting the small presence of aluminum (Al) along with the tungsten carbide (WC). The presence of aluminum over this region is because of the movement of the chips over the surface of the tool inserts while machining [34]. The presence of the aluminum being deposited on the worn-out tool insert is clearly shown in Table 5. The presence of aluminum deposition on the tool surface at the region of the yellow cross in Figure 6 is because of the formation of built-up edge (BUE) on the tool. The elemental composition of the same is also shown in Table 6.

A Rigaku brand Ultima IV was used to perform the X-ray diffraction (XRD) on the self-developed DLC coating on the tungsten carbide (WC) insert. It was performed in the 2θ range from 5° to 80° and the results are presented in Figure 7. As can be seen in the XRD profile of the coated WC tool in Figure 7, one visible peak is near 2θ~43.02° which matches the diamond {111} plane and the other peak at 2θ~75.52° which matched to the diamond {220} plane. All the other peaks originating in the X-ray diffraction spectra are from tungsten carbide WC substrate [35].
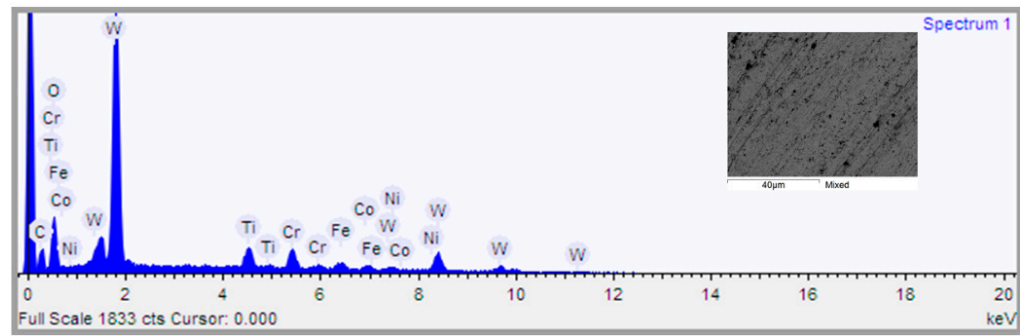
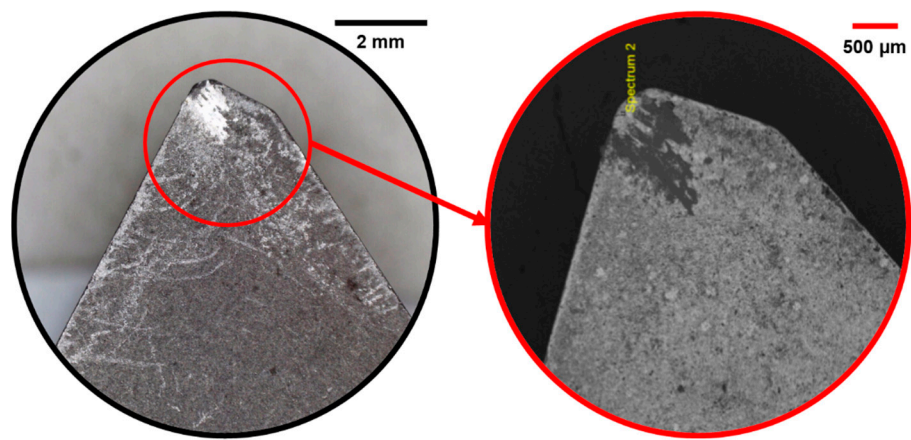**Figure 4.** EDaX spectrum of tungsten carbide (WC) substrate.

Figure 5. Wear of DLC-coated WC tool inserts shown on the microscopic image are encircled and the SEM image is shown on the right-hand side.

Table 4. Elemental composition of tungsten carbide (WC) substrate.

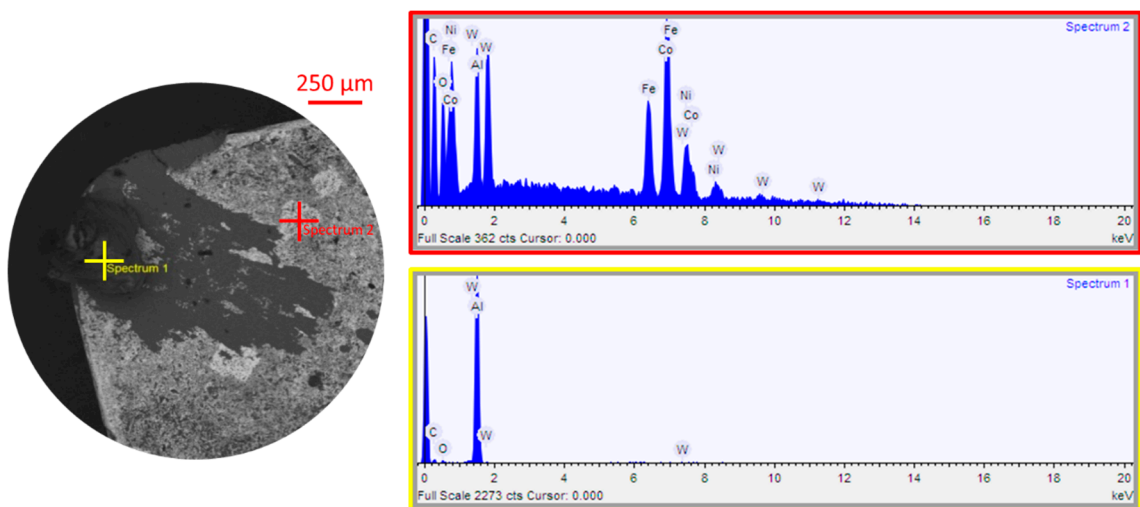| Element	W	C	O	Fe	Ti	Co	Ni	Cr
% Weight	44.18	17.46	14.53	8.82	4.27	3.86	3.34	2.27

Figure 6. EDaX spectrum of the built-up edge (BUE) formation on coated tungsten carbide (WC) tool inserts.

Table 5. Elemental composition of the red cross rectangular region in Figure 6.

Element	C	O	Al	Fe	Co	Ni	W
% Weight	24.18	8.79	3.64	12.18	7.84	11.28	32.09

Table 6. Elemental composition of the tool at the yellow cross in Figure 6.

Element	C	O	Si	Al	W
% Weight	32.39	5.29	0.32	60.43	1.57
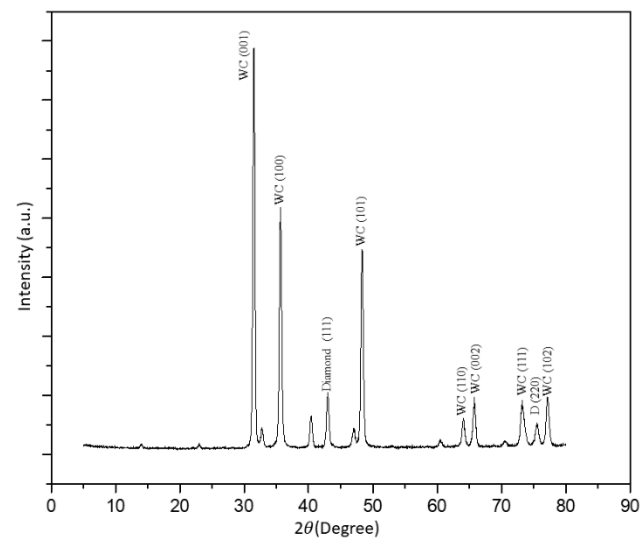
Figure 7. The X-ray diffraction spectra of the DLC-coated tungsten carbide tool.

3.2. Raman Spectrum

Diamond provides a single sharp peak of intensity at 1332 cm^{-1} because of its only active phonon [36]. A LabRAM Soleil™ Raman microscope was used to confirm the growth of the DLC coating by capturing the Raman spectra using a 514 nm lamp. Obtained Raman spectra for the same are shown in Figure 8. The obtained Raman spectra depicted that the D and G bands lie at 1338 cm^{-1} and 1576.5 cm^{-1} respectively. The sharp intensity of peak is observed at 1338 cm^{-1} in the spectrum, taken from the flat top surface of the coated tungsten carbide inserts. The center phonon mode of the as-developed DLC coating is the reason for the above-stated peak at 1338 cm^{-1}. It is observed from the Raman spectra that there is an upshift in the peak from 1332 cm^{-1} to 1338 cm^{-1}. This up-shift occurs because of the compressive stress developed on the as-developed DLC coating. The compressive stress developed because of the thermal stress, which was generated during the cooling process of the substrate to room temperature [13,18,21], which arises as a result of the mismatch in thermal coefficients of both diamond and tungsten carbide. The development of the G band at 1576.5 cm^{-1} was due to the co-existence of the sp2-phases, called trans-polyacetylene (trans-PA). Trans-PA is an alternate chain of sp2 carbon atoms, with a single hydrogen bonded to each carbon [37].
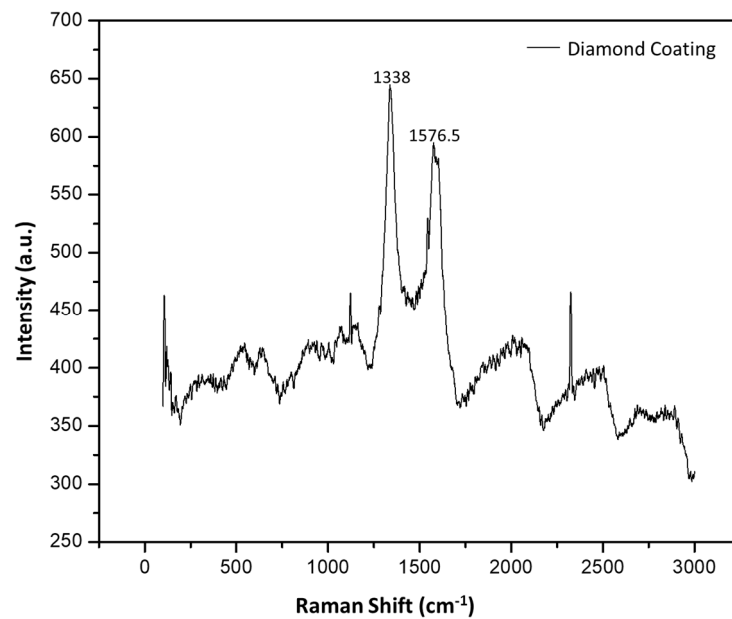
Figure 8. Raman spectra of the DLC-coated tungsten carbide tool inserts.

3.3. Hardness

A Fischerscope HM2000 (Fischer Measurement Technologies Pvt. Ltd., Pune/India) was used to perform the microhardness test on the coated and un-coated WC inserts. The method of partial loading and unloading on the surface for the measurement of hardness was used, which allowed the evaluation of adhesion of the self-deposited DLC coating on the WC substrate surface [17]. Figure 9 depicts the loading and unloading profile in the form of a graph obtained during the indentation testing process of measuring the hardness. The hardness was measured on the flank face of the tool insert before and after the coating process on the same WC substrate. Figure 9 shows one out of many measurement processes performed on the samples at various locations. The average evaluated Vickers hardness number after the various measurement processes were found to be 1478.78 HV and 953.95 HV for both DLC-coated tool inserts, as well as un-coated tool inserts, respectively. These values have been plotted and shown as a graph in Figure 10. The surface hardness values were measured by taking 4 measurements along the flank face of the tool insert before the coating process and then hardness was measured at the same flank face after the coating process. The applied tests have shown that the hardness of the un-coated WC inserts has been increased by a factor of 1.5 after the coating process. This shows that the life of the inserts has been enhanced by the coating process [38,39].
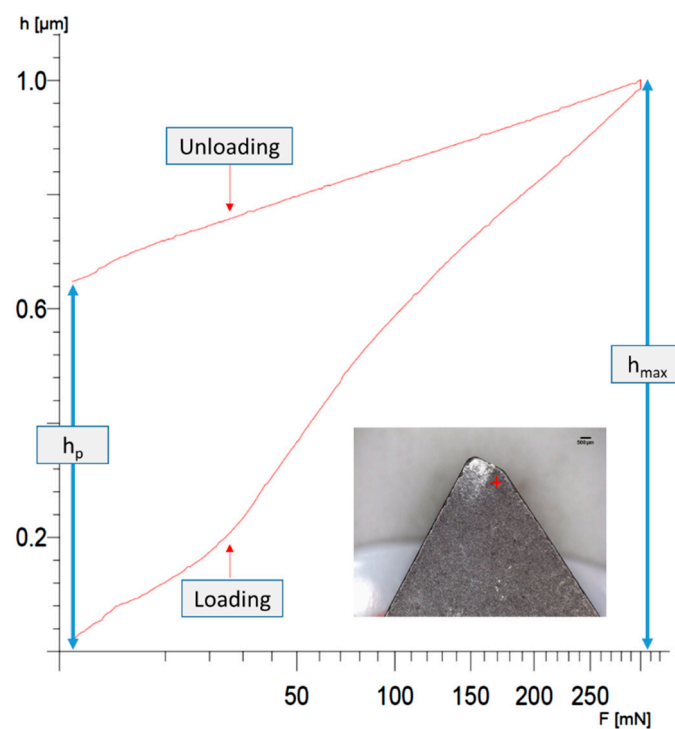
Figure 9. Loading and unloading profile graph obtained during the hardness measurement process.
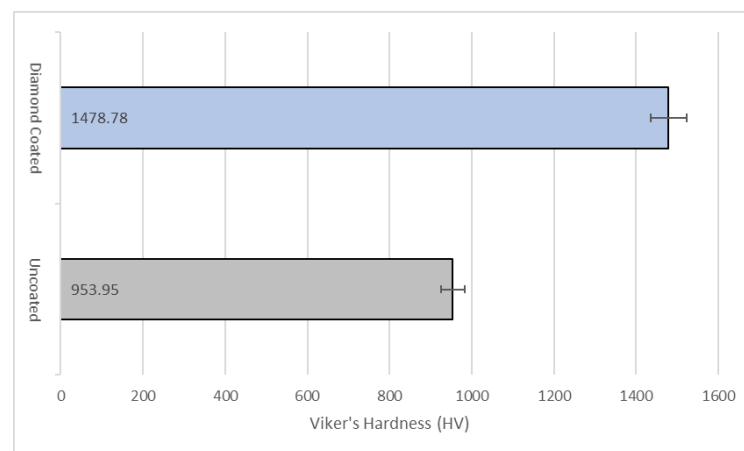

Figure 10. Average Vickers hardness values of the DLC-coated and un-coated WC tool inserts.

3.4. FESEM

An FEI Quanta 200 FESEM machine was used in the Institute Instrumentation Centre (IIC) of Indian Institutes of Technology Roorkee (IITR) for studying the morphology of the WC inserts before and after the growth of the DLC coating. The FESEM micrographs were captured at different magnifications. The quality of the as-developed DLC coating on the WC tool insert's surface was almost the same on the whole substrate. The presence of faceted growth of DLC can be seen in Figure 11 [15,40]. It is also clearly evident from the FESEM image in Figure 11 that the crystallites of the as-developed DLC coating get together to form clusters [17,41].
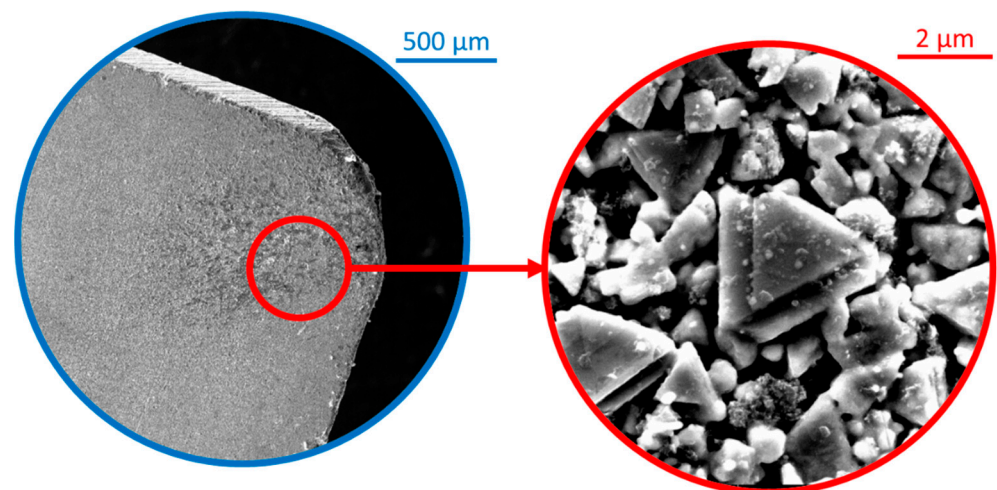
Figure 11. Faceted growth of DLC coating on the tungsten carbide (WC) tool inserts is encircled and enlarged.

4. Results and Discussion

This section provides a detailed results analysis using TOPSIS.

4.1. Selecting the Orthogonal Array (OA)

With the intention of deciding the optimum combination of the selected input parameters for decided response variables, we have used L_9 orthogonal array. Keeping the aim to find out the effect of input parameters viz. feed (f), cutting speed (V_c) and depth of cut (DOC) on the response variables (performance indicators) viz. flank wear, temperature in the cutting zone, and surface roughness, L_9 orthogonal array (OA) was selected. This was selected to have the least number of experimental runs.

These runs were computed by the following formula:

$$(L - 1)\,P + 1 \tag{1}$$

where, L: the levels in experimentation, and P: the number of parameters (P).

In this paper, we have used three input parameters (P = 3) having three levels (L = 3) for the experimentation. Hence, we opted for the L_9 orthogonal array shown in Table 7.

4.2. TOPSIS Based on Entropy Weight Method

To accomplish the optimal solution, we used a statistical tool. This method enlarges the distance from a negative ideal solution and also shortens the distance from a positive ideal solution. Moreover, this ranking method uses the closeness of the optimal solution from the positive ideal solution [41].

4.2.1. Formation of Decision Matrix

Using the responses, decision matrix A is formed. This decision matrix is evaluated for n responses of variables containing m of values [42]. The response variables in the form of an initial decision matrix are also shown in Table 7.

$$A = \left(a_{ij}\right)_{m \times n} = \begin{bmatrix} a_{11} & \cdots & a_{1n} \\ \vdots & \ddots & \vdots \\ a_{m1} & \cdots & a_{mn} \end{bmatrix} \tag{2}$$

Table 7. L$_9$ orthogonal array along with the response variables in the form of initial decision matrices.

Order of Experiment	Experiment No.	Input Parameters			(Response Variables)		
		DOC (mm)	Vc (m/min)	f (mm/rev)	Tc (°C)	Ra (µm)	Wf (µm)
8	1	0.375	480	0.125	72.8	0.565	96.25
5	2	0.375	600	0.25	80.0	0.491	100.67
1	3	0.375	720	0.375	79.6	0.64	113.33
9	4	0.635	480	0.25	79.3	0.389	85.33
6	5	0.635	600	0.375	133.6	0.558	86.25
7	6	0.635	720	0.125	112.2	0.319	94.25
4	7	0.895	480	0.375	160.4	0.482	96.25
2	8	0.895	600	0.125	167.7	0.46	103.75
3	9	0.895	720	0.25	202.0	0.467	115.42

4.2.2. Standardizing the Decision Matrix

To have the uniform units for all the responses viz. flank wear, temperature in the cutting zone, and surface roughness, we have standardized the decision matrix. In our paper, we have used the criterion of "lower the better" for all the responses. Table 8 shows the response variables in the form of the obtained standardized decision matrix.

If (a_{ij}) denotes the response variables for the lower the better standard.

$$(r_{ij}) = \frac{a_{ij}}{\sqrt{\sum_{i=1}^{n} a_{ij}^2}} \tag{3}$$

Consequently, evaluating the obtained standardized decision matrix by

$$R = (r_{ij})_{m+n} \tag{4}$$

4.2.3. Using the Entropy Method for the Determining the Weight for Response Variable

The entropy technique was used for calculating the weight for all the response variables. The calculation for the entropy of the performance indicator for the jth response variable is done by:

$$e_j = -k \sum_{i}^{m} r_{ij \; lnr_{ij}}, \; j = 1, 2, \ldots, n \; and \tag{5}$$

$$k = \frac{1}{\ln(m)} \tag{6}$$

Calculation of the performance indicator's total entropy done by:

$$E = -\frac{1}{\ln(m)} \cdot \sum_{j=1}^{n} \sum_{i=1}^{m} r_{ij} ln(r_{ij}) \tag{7}$$

Calculation of the inequality for jth response variable is done by:

$$d_j = |1 - e_j|, \; j = 1, 2, 3, \ldots n \tag{8}$$

Table 8. Response variables in the form of obtained standardized decision matrix.

Run No.	Performance Indicators (Response Variables)		
	Tc	*Ra*	*Wf*
1	0.1883	0.3812	0.3223
2	0.2070	0.3313	0.3371
3	0.2059	0.4318	0.3795
4	0.2052	0.2625	0.2857
5	0.3456	0.3765	0.2888
6	0.2903	0.2152	0.3156
7	0.4150	0.3252	0.3223
8	0.4338	0.3104	0.3474
9	0.5226	0.3151	0.3865

Whenever d_j is larger, r_{ij} will be propagated more, which, in turn, will make response variable "j" the important one. Similarly, when r_{ij}, becomes comparatively saturated, it makes "j" the least important response variable.

Calculation of the weight factor was done by:

$$w_j = d_j / \sum_{j=1}^{n} d_j \tag{9}$$

4.2.4. Determination of Weight

R = standardized decision matrix = $(r_{ij})_{m \times n}$,

w_j = calculated weight of the evaluated responses,

The weighted decision matrix of all the response variables was calculated by the following matrix and is shown in Table 10:

$$v = \begin{bmatrix} w_1 r_{11} & w_2 r_{12} \cdots & w_n r_{1n} \\ \vdots & \ddots & \vdots \\ w_1 r_{m1} & w_2 r_{m2} \cdots & w_n r_{mn} \end{bmatrix} = \begin{bmatrix} v_{11} & v_{12} \cdots & v_{1n} \\ \vdots & \ddots & \vdots \\ v_{m1} & v_{m2} \cdots & v_{mn} \end{bmatrix} \tag{10}$$

Weights of the evaluated responses are shown in Table 9.

Table 9. Weights of the performance indicators.

Tc	*Ra*	*Wf*
0.2945	0.3459	0.3596

Table 10. Performance indicator's standardized and weighted decision matrices.

Run No.	*Tc*	*Ra*	*Wf*
1	0.055465	0.131862	0.115897
2	0.060951	0.114591	0.121219
3	0.060646	0.149365	0.136464
4	0.060418	0.090786	0.102748
5	0.101788	0.130228	0.103856
6	0.085484	0.074449	0.113489
7	0.122207	0.112491	0.115897
8	0.127768	0.107356	0.124928
9	0.153901	0.108990	0.138977

4.2.5. Calculation for Finding the Negative and Positive Ideal Solution

The expression used for determining the positive ideal solution is mentioned below:

$$V^+ = \left\{ v_1^+, v_2^+, \cdots\cdots, v_n^+ \right\} = \left\{ \left(max \; v_{ij} \middle| j \varepsilon J_1 \right), \left(min \; v_{ij} \middle| j \varepsilon J_2 \right) \middle| i = 1, 2, \cdots\cdots, m \right\} \quad (11)$$

The expression used for determining the negative ideal solution is mentioned below:

$$V^- = \left\{ v_1^-, v_2^-, \cdots\cdots, v_n^- \right\} = \left\{ \left(min \; v_{ij} \middle| j \varepsilon J_1 \right), \left(max \; v_{ij} \middle| j \varepsilon J_2 \right) \middle| i = 1, 2, \cdots\cdots, m \right\} \quad (12)$$

where J_1 = variable for larger the better; J_2 = variable for smaller the better.

4.2.6. Determination of the Relative Distance

$$S_i^+ = \sqrt{\sum_{i=1}^{n} \left(v_{ij} - v_j^+ \right)^2}, \; i = 1, 2, 3, \ldots., m \quad (13)$$

$$S_i^- = \sqrt{\sum_{i=1}^{n} \left(v_{ij} - v_j^- \right)^2}, \; i = 1, 2, 3, \ldots., m \quad (14)$$

where, S_i^+ = relative distance between V_{ij} and positive ideal solution V_j^+, S_i^- = relative distance between V_{ij} and negative ideal solution V_j^-.

The relative distance of the considered performance indicators is shown in Table 11.

4.2.7. Formation of Sequence Table While Evaluating the TOPSIS Value

Calculated preferred values "C_j" and assigned ranks of the experimental values are also shown in Table 11.

$$C_j = S_i^- / \left(S_i^+ + S_i^+ \right) \quad (15)$$

Table 11. Standardized and weighted decision matrices for performance indicators.

Run No.	S_i^+	S_i^-	C_j	Rank
1	0.058898823	0.10260916	0.635319432	4
2	0.04452703	0.100818111	0.693646246	3
3	0.082316442	0.093288765	0.531241449	5
4	0.017070944	0.116117165	0.87182832	1
5	0.072513964	0.065692309	0.475320746	6
6	0.031882051	0.104608721	0.766416068	2
7	0.07793875	0.053823209	0.408488227	7
8	0.08247761	0.051429923	0.384070423	8
9	0.110431731	0.040375324	0.267728348	9

4.3. Discussion

To optimize the selected input parameters of the turning process for the self-developed DLC-coated tungsten carbide (WC) tool inserts, while using the TOPSIS method, is the main objective of our paper. According to the TOPSIS (technique for order of preference by similarity to ideal solution) method, there should be a maximum value of the relative closeness for obtaining the optimum cutting conditions [23]. In this paper, for obtaining the optimal performance of the machining process, the minimization characteristic for temperature in the cutting zone (Tc), surface roughness (Ra), and flank wear (Wf) was taken [32–34]. As already mentioned, the obtained results are shown in Table 8. As also mentioned in Section 4.2.6, the minimum values of temperature in the cutting zone (Tc), surface roughness (Ra), and flank wear (Wf) are indicated by the maximum relative closeness [40]. The values of 0.635 mm depth of cut, feed rate of 0.25 mm/rev, and cutting speed of 480 m/min are the optimal values of input parameters for achieving the minimum values of response variables using the DLC-coated tungsten carbide (WC) tool inserts in a turning process [4,17].

The optimum value indicates that with the lower level of feed, depth of cut, and cutting speed, we can reduce the surface roughness and tool flank wear along with the temperature in the cutting zone. At the lower level of input parameters, the minimum values of response variables are achieved because of the smaller co-efficient of friction [15]. As, compared to other methods, such as the artificial neural network (ANN) and genetic algorithm (GA), the TOPSIS (a technique for the order of preference by similarity to ideal solution) method has less computational steps [15].

5. Conclusions

In this paper, the DLC coating was developed on the tungsten carbide (WC) tool insert to minimize the selected response variables viz. flank wear, temperature in the cutting zone, and surface roughness. From this study, the following conclusions were drawn:

(a) X-ray diffraction spectra for the coated tungsten carbide substrate confirmed the presence of DLC coating developed on tungsten carbide (WC) substrate.

(b) The peak at 1338 cm^{-1} in the Raman spectra also supported the presence of DLC coating on tungsten carbide (WC) inserts. The result of the presence of DLC is in correlation with the SEM images.

(c) It was also observed that the hardness of the WC was increased by a factor of 1.5 after the coating process. The average Vickers hardness was 953.95 HV for the un-coated tungsten carbide (WC) and for the DLC-coated WC, the hardness increased to 1478.78 HV.

(d) The optimum value of depth of cut for achieving the minimum value of the selected response variables using the self-developed DLC-coated tungsten carbide (WC) tool inserts in a turning process, was found to be 0.635 mm.

(e) The optimum values of cutting speed and feed for achieving the minimum value of the selected response variables using the self-developed DLC-coated tungsten carbide (WC) tool inserts in a turning process, were found to be 480 m/min and 0.25 mm/rev respectively.

Nomenclature

WC	Tungsten Carbide
CVD	Chemical Vapor Deposition
DLC	Diamond-like Carbon
DOC	Depth of Cut
T_c	Temperature in the Cutting Zone
p-SBg	Pyrolyzed Sugarcane Bagasse
FESEM	Field Emission Scanning Electron Microscope
f	Feed
R_a	Surface Roughness
V_c	Cutting Speed
XRD	X-ray Diffraction
SBg	Sugarcane Bagasse

References

1. Tanaka, T.; Akasawa, T. Machinability of Hypereutectic Silicon-Aluminum Alloys. *J. Mater. Eng. Perform.* **1999**, *8*, 463–468. [CrossRef]
2. Boyer, R.; Cotton, J.; Mohaghegh, M.; Schafrik, R. Materials considerations for aerospace applications. *MRS Bull.* **2015**, *40*, 1055–1066. [CrossRef]
3. Ed, F.; Chris, E. Basics of CVD Diamond-Coated Cutting Tools. American Mold Builder. 2017. Available online: https://americanmoldbuilder.com/articles/2017/basics-of-cvd-diamond-coated-cutting-tools/ (accessed on 12 February 2021).
4. Kumar, C.S.; Majumder, H.; Khan, A.; Patel, S.K. Applicability of DLC and WC/C low friction coatings on Al_2O_3/TiCN mixed ceramic cutting tools for dry machining of hardened 52100 steel. *Ceram. Int.* **2020**, *46*, 11889–11897. [CrossRef]
5. Aschauer, E.; Riedl, H.; Koller, C.; Bolvardi, H.; Arndt, M.; Polcik, P.; Mayrhofer, P. Adhesive wear formation on PVD coated tools applied in hot forming of Al-Si coated steel sheets. *Wear* **2019**, *430-431*, 309–316. [CrossRef]
6. Evaristo, M.; Fernandes, F.; Cavaleiro, A. Room and High Temperature Tribological Behaviour of W-DLC Coatings Produced by DCMS and Hybrid DCMS-HiPIMS Configuration. *Coatings* **2020**, *10*, 319. [CrossRef]
7. Grácio, J.; Fan, Q.H.; Madaleno, J.C. Diamond growth by chemical vapour deposition. *J. Phys. D Appl. Phys.* **2010**, *43*, 374017. [CrossRef]
8. Srinivasan, B.; Rao, M.S.R.; Rao, B.C. On the development of a dual-layered diamond-coated tool for the effective machining of titanium Ti-6Al-4V alloy. *J. Phys. D Appl. Phys.* **2017**, *50*, 015302. [CrossRef]
9. Asmussen, J.; Reinhard, D. *Diamond Films Handbook*; CRC Press: Boca Raton, FL, USA, 2002.
10. Erdemir, A.; Martin, J.M. Superior wear resistance of diamond and DLC coatings. *Curr. Opin. Solid State Mater. Sci.* **2018**, *22*, 243–254. [CrossRef]
11. Mustafi, L.; Rahman, M.M.; E Alam Al Nasim, M.N.; Chowdhury, M.A.; Monir, M.H. Deposition behavior and tribological properties of diamond-like carbon coatings on stainless steels via chemical vapor deposition. *Int. J. Miner. Met. Mater.* **2018**, *25*, 1335–1343. [CrossRef]
12. Urakami, N.; Kosaka, M.; Hashimoto, Y. Thermal chemical vapor deposition and luminescence property of graphitic carbon nitride film for carbon-based semiconductor systems. *Jpn. J. Appl. Phys.* **2018**, *58*, 010907. [CrossRef]
13. Wang, J.; Ma, J.; Huang, W.; Wang, L.; He, H.; Liu, C. The investigation of the structures and tribological properties of F-DLC coatings deposited on Ti-6Al-4V alloys. *Surf. Coat. Technol.* **2017**, *316*, 22–29. [CrossRef]
14. E Bobylyov, E.; Storozhenko, I.D. Diffusion metallization of carbide cutting tools as a way to improve the surface treatment quality. *J. Phys. Conf. Ser.* **2019**, *1399*, 044084. [CrossRef]
15. Rana, R.; Murtaza, Q.; Walia, R. GA based optimization of tri-bological behaviour of diamond coated tungsten carbide. *World J. Eng.* **2020**, *17*, 335–346. [CrossRef]
16. Radziejewska, J.; Psiuk, R.; Mościcki, T. Characterization and Wear Response of Magnetron Sputtered W–B and W–Ti–B Coatings on WC–Co Tools. *Coatings* **2020**, *10*, 1231. [CrossRef]
17. D'Orazio, A.; El Mehtedi, M.; Forcellese, A.; Nardinocchi, A.; Simoncini, M. Tool wear and hole quality in drilling of CFRP/AA7075 stacks with DLC and nanocomposite TiAlN coated tools. *J. Manuf. Process.* **2017**, *30*, 582–592. [CrossRef]
18. Krishnia, L.; Tyagi, P.K. Growth and characterization of polycrystalline diamond films on silicon using sugarcane bagasse as carbon precursor at atmospheric pressure by thermal chemical vapor deposition. *Diam. Relat. Mater.* **2018**, *87*, 18–26. [CrossRef]
19. Mohtashami, S.-A.; Kolur, N.A.; Kaghazchi, T.; Asadi-Kesheh, R.; Soleimani, M. Optimization of sugarcane bagasse activation to achieve adsorbent with high affinity towards phenol. *Turk. J. Chem.* **2018**, *42*, 1720–1735. [CrossRef]
20. Krishnia, L.; Yadav, B.S.; Palnitkar, U.; Satyam, P.; Gupta, B.K.; Koratkar, N.A.; Tyagi, P.K. As-pyrolyzed sugarcane bagasse possessing exotic field emission properties. *Appl. Surf. Sci.* **2018**, *443*, 184–190. [CrossRef]
21. Rao, R.V. Machinability evaluation of work materials using a combined multiple attribute decision-making method. *Int. J. Adv. Manuf. Technol.* **2006**, *28*, 221–227. [CrossRef]

22. Thirumalai, R.; Senthilkumaar, J.S. Multi-criteria decision making in the selection of machining parameters for Inconel 718. *J. Mech. Sci. Technol.* **2013**, *27*, 1109–1116. [CrossRef]

23. Balasubramaniyan, S.; Selvaraj, T. Application of integrated Taguchi and TOPSIS method for optimization of process parameters for dimensional accuracy in turning of EN25 steel. *J. Chin. Inst. Eng.* **2017**, *40*, 267–274. [CrossRef]

24. Huang, L.; Yuan, J.; Li, C.; Hong, D. Microstructure, tribological and cutting performance of Ti-DLC/α-C:H multilayer film on cemented carbide. *Surf. Coat. Technol.* **2018**, *353*, 163–170. [CrossRef]

25. Adalarasan, R.; Sundaram, A.S. Parameter design and analysis in continuous drive friction welding of Al6061/SiCp composites. *J. Mech. Sci. Technol.* **2015**, *29*, 769–776. [CrossRef]

26. Tyagi, A.; Walia, R.; Murtaza, Q. Tribological behavior of temperature dependent environment friendly thermal CVD diamond coating. *Diam. Relat. Mater.* **2019**, *96*, 148–159. [CrossRef]

27. Hess, P. The mechanical properties of various chemical vapor deposition diamond structures compared to the ideal single crystal. *J. Appl. Phys.* **2012**, *111*, 051101. [CrossRef]

28. Jaguaribe, E.F.; Medeiros, L.L.; Barreto, M.C.S.; Araujo, L.P. The performance of activated carbons from sugarcane bagasse, babassu, and coconut shells in removing residual chlorine. *Braz. J. Chem. Eng.* **2005**, *22*, 41–47. [CrossRef]

29. Rana, R.; Murtaza, Q.; Walia, R.S. Optimization using genetic algorithm of tribological behaviour of wc tool material. *Indian J. Eng. Mater. Sci.* **2020**, *27*, 889–896.

30. Lal, R.; Singh, R. Investigations of tribodynamic characteristics of chrome steel pin against plain and textured surface cast iron discs in lubricated conditions. *World J. Eng.* **2019**, *16*, 560–568. [CrossRef]

31. Sahithi, V.V.D.; Malayadrib, T.; Srilatha, N. Optimization of Turning Parameters on Surface Roughness Based on Taguchi Technique. *Mater. Today: Proc.* **2019**, *18*, 3657–3666. [CrossRef]

32. Jamil, M.; Khan, A.M.; He, N.; Li, A.; Zhao, W.; Sarfraz, S. Multi-response optimisation of machining aluminium-6061 under eco-friendly electrostatic minimum quantity lubrication environment. *Int. J. Mach. Mach. Mater.* **2019**, *21*, 459. [CrossRef]

33. Prakash, K.S.; Gopal, P.; Karthik, S. Multi-objective optimization using Taguchi based grey relational analysis in turning of Rock dust reinforced Aluminum MMC. *Measurement* **2020**, *157*, 107664. [CrossRef]

34. Niknam, S.A.; Jalali, A. Effects of lubricants and flow rates on the surface roughness and chip thickness when MQL turning of aero-engine aluminum alloys 6061-T6 and 7076-T6. *Int. J. Adv. Manuf. Technol.* **2020**, *110*, 1–8. [CrossRef]

35. Abbas, A.T.; Pimenov, D.Y.; Erdakov, I.; Taha, M.A.; El Rayes, M.M.; Soliman, M.S. Artificial intelligence monitoring of hardening methods and cutting conditions and their effects on surface roughness, performance, and finish turning costs of solid-state recycled aluminum alloy 6061 chips. *Metals* **2018**, *8*, 394. [CrossRef]

36. Rachedi, N.; Hadjersi, T.; Moulai, F.; Dokhane, N.; Manseri, A.; Bouanik, S. Effect of Electrolyte Type on Properties of Diamond-like Carbon Films Electrodeposited onto N-Type Si Substrate, Application as Electrode for Supercapacitors. *Silicon* **2019**, *12*, 2445–2453. [CrossRef]

37. Ferrari, A.C.; Robertson, J. Origin of the 1150-cm^{-1}. Raman mode in nanocrystalline diamond. *Phys. Rev. B* **2001**, *63*, 121405. [CrossRef]

38. Kong, J.; Xing, P.; Liu, Y.; Wang, J.; Jin, X.; Feng, Z.; Luo, X. An Economical Approach for the Recycling of High-Purity Silicon from Diamond-Wire Saw Kerf Slurry Waste. *Silicon* **2018**, *11*, 367–376. [CrossRef]

39. Sarangi, S.; Chattopadhyay, A. Effect of pretreatment methods and chamber pressure on morphology, quality and adhesion of HFCVD diamond coating on cemented carbide inserts. *Appl. Surf. Sci.* **2008**, *254*, 3721–3733. [CrossRef]

40. Ghadai, R.K.; Das, S.; Kalita, K.; Swain, B.P.; Davim, J.P. Structural and Mechanical Analysis of APCVD Deposited Diamond-Like Carbon Thin Films. *Silicon* **2020**, 1–10. [CrossRef]

41. Knight, D.S.; White, W.B. Characterization of diamond films by Raman spectroscopy. *J. Mater. Res.* **1989**, *4*, 385–393. [CrossRef]

42. Tiwari, D.; Sherwani, A.F.; Muqeem, M.; Goyal, A. Parametric optimization of organic Rankine cycle using TOPSIS integrated with entropy weight method. *Energy Sources Part A Recover. Util. Environ. Eff.* **2019**, 1–18. [CrossRef]